Casimir effect in critical systems: A Monte Carlo simulation

M. Krech and D. P. Landau
Center for Simulational Physics, The University of Georgia, Athens, Georgia 30602
(Received 22 September 1995)

If a critical system is confined to a finite geometry, critical fluctuations of the order parameter generate long-ranged forces between the system boundaries. These forces, commonly known as Casimir forces, are characterized by universal amplitudes and scaling functions. A hybrid Monte Carlo algorithm has been devised and used to measure the Casimir amplitudes directly and accurately. We apply the algorithm to a critical q-state Potts model confined to a rectangular $M\times L$ geometry in $d=2$ dimensions and to a critical Ising model confined to a $M^2\times L$ geometry in $d=3$ dimensions. We find good agreement with rigorous results in $d=2$ and compare our results with field-theoretic estimates of the Casimir amplitude in $d=3$.

PACS number(s): 64.60.Fr, 05.70.Jk, 68.35.Rh

I. INTRODUCTION

One of the most fundamental discoveries in the theory of electromagnetism dates back to the year 1948, when the Dutch physicist H. B. G. Casimir realized that two metallic plates placed parallel to one another at a distance L in vacuum experience an attractive force [1]. According to the modern view of this effect, which had also been proposed by Casimir, the metallic plates impose boundary conditions on the *zero-point* fluctuations of the electromagnetic field thereby imposing an L dependence on the fluctuation spectrum. This in turn gives rise to an L dependence in the total *energy* E of the configuration. Likewise, *thermal* fluctuations of the electromagnetic field at high temperatures introduce a similar L dependence to the configuration energy [2]. Specifically, in the limit of large cross-section areas A of the plates one obtains [1,2]

$$\lim_{A\to\infty}\frac{E}{A}=-\frac{\pi^2}{720}\frac{\hbar c}{L^3},\quad T=0$$

$$\lim_{A\to\infty}\frac{E}{A}=-\frac{\zeta(3)}{8\pi}\frac{k_BT}{L^2},\quad k_BT\gg\frac{\hbar c}{L} \tag{1.1}$$

where $\zeta(3)\simeq 1.202$ is a special value of the Riemann ζ function. Note, that the dimensionless amplitudes in Eq. (1.1) are given by the corresponding amplitude $\Delta=-2^{-d}\pi^{-d/2}N\Gamma(d/2)\zeta(d)$ of a massless (i.e., critical) Gaussian field theory [3,4] for $N=2$ components in $d=4$ and $d=3$ dimensions, respectively.

Several years after Casimir's discovery a general theory of these so-called dispersion forces in layered dielectrics was formulated [5] yielding a unified picture of the Casimir forces and the well known van der Waals forces [6]. It was already noted in Ref. [5] that the dispersion forces play an important role in the vast realm of the wetting phenomena [7]. In the simplest case a wetting transition leads to the formation of a macroscopically thick liquid layer on the surface of a homogeneous plane substrate which is exposed to the vapor of the wetting agent. The combined substrate-liquid-vapor system then has the structure of the layered dielectrics considered in Ref. [5]. The equilibrium thickness of the wetting layer is determined by the minimum of the so-called effective interface potential Ω as function of a *prescribed* thickness l [7]

$$\lim_{A\to\infty}\frac{\Omega(T,l)}{A}=\omega(l)=l[\rho_l(T)/\rho_v(T)-1]p_0(T)\delta p+\sigma_{sl}(T)+\sigma_{lv}(T)+\delta\omega(T,l), \tag{1.2}$$

where A is the interfacial area, $\rho_l(T)$ and $\rho_v(T)$ denote the liquid and the vapor density, respectively, $p_0(T)$ is the vapor pressure *at* liquid-vapor coexistence, and δp is a dimensionless measure of the undersaturation of the vapor. The substrate-liquid and liquid-vapor interfacial tensions $\sigma_{sl}(T)$ and $\sigma_{lv}(T)$ do not depend on l, and $\delta\omega(T,l)$ contains the contribution of the van der Waals forces which has the asymptotic form [8]

$$\delta\omega_{vdW}(l)=\begin{cases}Wl^{-2}+\mathcal{O}(l^{-3}) & \text{(nonretarded)}\\ W_rl^{-3}+\mathcal{O}(l^{-4}) & \text{(retarded)},\end{cases} \tag{1.3}$$

where the weak temperature dependence of the Hamaker constants W and W_r has been disregarded. Note, that according to Eq. (1.2) with $\delta\omega(l)=\delta\omega_{vdW}(l)$ one obtains $L\propto(\delta p)^{-1/3}$ for the equilibrium thickness L for the nonretarded van der Waals forces. This power law crosses over to $L\propto(\delta p)^{-1/4}$ for $\delta p\to 0$ because the van der Waals forces become retarded as L increases.

According to the mechanism underlying the Casimir effect in electromagnetism, critical fluctuations of the order parameter at a critical point of a wetting agent generate an additional long-ranged force which contributes to $\delta\omega(l)$ [see Eq. (1.2)]. One finds [9]

$$\delta\omega(T_c,l)=\delta\omega_{vdW}(l)+k_BT_c\Delta l^{-(d-1)} \tag{1.4}$$

in d dimensions, where Δ is the *universal* Casimir amplitude, and T_c is the critical temperature. Therefore one expects a critical effect on the equilibrium layer thickness L, e.g., in the vicinity of the λ transition in ^{4}He [10] and near critical points of the demixing transition in the binary mixtures [11,12]. The Casimir amplitude Δ in Eq. (1.4) is exactly known for the critical Ising and three-state Potts models in

$d=2$ dimensions [13]. However, in $d=3$, which is the experimentally relevant case, Δ can only be estimated [9,14].

We have devised a hybrid Monte Carlo algorithm which allows us to measure the Casimir amplitude Δ of a critical lattice model *directly* with considerable accuracy. The availability of rigorous results for Δ for the critical q-state Potts model in $d=2$ for $q=2$ and $q=3$ for all possible boundary conditions [13] provides the testing ground for the Monte Carlo algorithm presented here. For this purpose we restrict ourselves to the case of cyclic, i.e., closed boundary conditions, for which the free energy does not contain surface contributions [see Eq. (1.2)]. The presence of surface contributions to the free energy especially in the case of applied surface fields requires additional customization of the algorithm which will not be discussed here.

The remainder of this paper is organized as follows. In Sec. II we present the lattice models we use for the simulation and give a detailed account of the Monte Carlo algorithm. Section III is devoted to the application of the algorithm to the critical q-state Potts model for $q=2$, 3, and 4 in a rectangular geometry for various aspect ratios in $d=2$. In Sec. IV we present the first results for the critical Ising model confined to a slab geometry in $d=3$. Finally we summarize our results in Sec. V.

II. LATTICE MODELS AND MONTE CARLO METHOD

For our investigation of the Casimir effect in two-dimensional critical systems belonging to the q-state Potts universality class we consider the ferromagnetic q-state Potts model with nearest neighbor interactions on a square lattice without external fields. Using the standard Kronecker-δ representation for the interaction between neighboring Potts spins $\sigma(\mathbf{r})$ and $\sigma(\mathbf{r}')$ we may write the model Hamiltonian as

$$\mathscr{H}\{\sigma\}=-J\sum_{\langle \mathbf{r},\mathbf{r}'\rangle}\delta_{\sigma(\mathbf{r}),\sigma(\mathbf{r}')}, \tag{2.1}$$

where $\mathbf{r}=(x,y)$, $\mathbf{r}'=(x',y')$ denote lattice sites and $\sigma(\mathbf{r})\in\{1,2,...,q\}$. The coupling constant J is positive and the angular brackets $\langle \mathbf{r},\mathbf{r}'\rangle$ denote a nearest neighbor pair. The geometry of the lattice underlying Eq. (2.1) is chosen to be rectangular with $M\times L$ lattice sites and $M\geqslant L$. Along the x direction we always apply periodic boundary conditions, i.e., the spins $\sigma(M,y)$ and $\sigma(1,y)$ are treated as nearest neighbor pairs with the interaction strength J. Along the y direction the boundary conditions are varied according to the case under consideration. The critical point of the ferromagnetic q-state Potts model on an infinite square lattice is located at its self-dual point, which for the model defined by Eq. (2.1) is given by [15]

$$(e^{K_c}-1)^2=q, \tag{2.2}$$

where $K_c=J/(k_BT_c)$ and T_c denotes the critical temperature.

In the three-dimensional case we consider the ferromagnetic spin-$\frac{1}{2}$ Ising model on a simple cubic lattice with nearest neighbor interaction, which is the standard representative of the Ising universality class. In the absence of external fields we use the Hamiltonian in the form

$$\mathscr{H}\{\sigma\}=-J\sum_{\langle \mathbf{r},\mathbf{r}'\rangle}\sigma(\mathbf{r})\sigma(\mathbf{r}'), \tag{2.3}$$

where $\mathbf{r}=(x,y,z)$, $\mathbf{r}'=(x',y',z')$ denote the lattice sites and $\sigma(\mathbf{r})=\pm 1$ for convenience. The geometry of the lattice underlying Eq. (2.3) is a slab containing $M^2\times L$ lattice sites and $M\geqslant L$. Along the x and y direction we always apply periodic boundary conditions in the same sense as described above. The boundary conditions along the z direction vary according to the situation to be studied. The position of the critical point of the model defined by Eq. (2.3) on an infinite simple cubic lattice has been conjectured to be given by [16]

$$\tanh K_c=(\sqrt{5}-2)\cos\frac{\pi}{8}, \tag{2.4}$$

where K_c is defined as in Eq. (2.2). The critical temperature according to Eq. (2.4) is given by $K_c=0.221\,658\,6...$ which agrees to within five to six digits with the estimates for K_c from the series expansions and recent Monte Carlo simulations [17].

There have been several previous attempts to access the critical finite-size amplitudes by Monte Carlo simulations [18,19] (see Ref. [20] for a detailed review). In the most recent one [19] the critical finite-size amplitude of the free energy of an Ising model has been related to the order parameter distribution function, which can be probed directly by Monte Carlo simulations. In Ref. [19] a cubic geometry, i.e., $M=L$ with purely periodic boundary conditions has been used. In order to investigate the rectangular or the slab geometry on which we will focus here, we have basically followed the approach outlined in Ref. [18], where the geometry itself is changed as a function of a parameter λ in order to probe the corresponding change of the free energy directly. In the case of the critical Potts model in the rectangular geometry in $d=2$ and even values of L this is accomplished by introducing a seam Hamiltonian $\mathscr{H}_{\rm seam}\{\sigma\}$ between the two rows of spins at $y=\frac{1}{2}L$ and $y=\frac{1}{2}L+1$ such that the *combined* Hamiltonian $\mathscr{H}\{\sigma\}+\mathscr{H}_{\rm seam}\{\sigma\}$ describes two uncoupled Potts models, each on a square lattice with $M\times\frac{1}{2}L$ sites. One of these subsystems is endowed with periodic boundary conditions along the y direction whereas the other inherits the boundary conditions of the initial system described by Eq. (2.1). The interpolating Hamiltonian

$$\mathscr{H}_\lambda\{\sigma\}=\mathscr{H}\{\sigma\}+\lambda.\mathscr{H}_{\rm seam}\{\sigma\}, \tag{2.5}$$

for $0\leqslant\lambda\leqslant 1$ then describes all the intermediate stages in the process of splitting the system into two decoupled subsystems. This procedure is graphically displayed in Fig. 1 showing the initial lattice model described by $\mathscr{H}_0\{\sigma\}=\mathscr{H}\{\sigma\}$ [see Eqs. (2.1) and (2.5)], an intermediate stage described by $\mathscr{H}_\lambda\{\sigma\}$ according to Eq. (2.5) for $0<\lambda<1$ with additional far reaching bonds, and the final stage described by Eq. (2.5) for $\lambda=1$. The explicit construction of the seam Hamiltonian $\mathscr{H}_{\rm seam}\{\sigma\}$ is very simple, so that we only quote its form for the case of periodic boundary conditions along the y direction. It reads

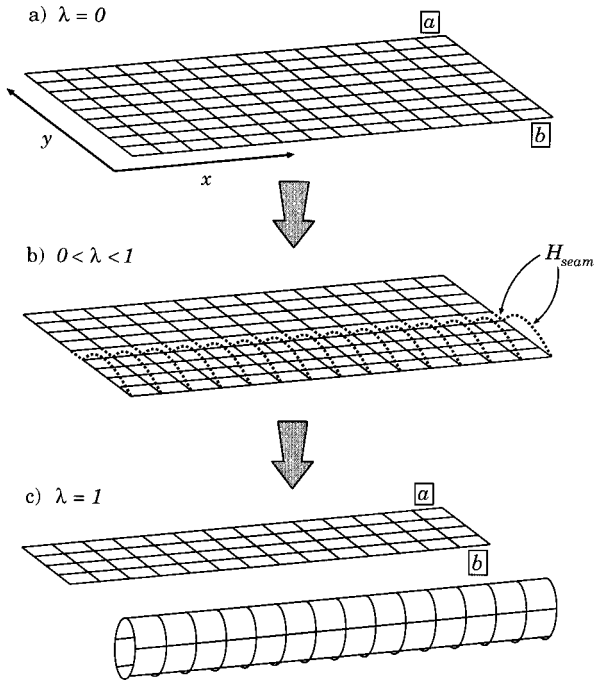

FIG. 1. Splitting procedure for the lattice. All lattices are closed periodically along the x direction (not shown). (a) Initial stage ($\lambda=0$). The labels a and b indicate that the boundary conditions of type $\boxed{a}$ and $\boxed{b}$, respectively, are applied across the lattice in the y direction. The Hamiltonian of the system is given by Eq. (2.1) ($d=2$) or Eq. (2.3) ($d=3$). (b) Intermediate stage ($0<\lambda<1$). The dotted lines indicate additional bonds introduced into the system by the seam Hamiltonian $\mathscr{H}_{\rm seam}$. The Hamiltonian of the system is given by Eq. (2.5). (c) Final stage ($\lambda=1$). The lattice is split into two decoupled subsystems, one with the old boundary conditions a and b, the other with periodic boundary conditions in the y direction indicated by its cylindrical shape.

$$\mathscr{H}_{\rm seam}\{\sigma\}=J\sum_{x=1}^{M}[\,\delta_{\sigma(x,L/2),\sigma(x,L/2+1)}+\delta_{\sigma(x,1),\sigma(x,L)}-\delta_{\sigma(x,1),\sigma(x,L/2)}-\delta_{\sigma(x,L/2+1),\sigma(x,L)}]. \quad (2.6)$$

For the Ising model in $d=3$ the corresponding seam Hamiltonian is the natural three dimensional extension of Eq. (2.6), where only the interactions have to be replaced according to Eq. (2.3).

The change in the free energy $\mathscr{F}$ at $T=T_c$, which corresponds to the change in the geometry for $\lambda=1$ compared to $\lambda=0$ (see Fig. 1), follows directly from elementary statistical mechanics. It is given by

$$\mathscr{F}\{\mathscr{H}+\mathscr{H}_{\rm seam}\}-\mathscr{F}\{\mathscr{H}\}=-k_BT_c\,\ln\langle\exp(-\mathscr{H}_{\rm seam}/k_BT_c)\rangle_{\mathscr{H}}, \quad (2.7)$$

where $\langle\cdots\rangle_{\mathscr{H}}$ denotes the thermal average with respect to the Hamiltonian $\mathscr{H}$ of the initial Potts model. In the limit of the vanishing aspect ratio $s=M/L$ either of the free energies $\mathscr{F}$ in Eq. (2.7) can be written in the form of Eq. (1.2) with Ω replaced by $\mathscr{F}$ and A replaced by M in $d=2$ and by M^2 in $d=3$. According to the choice of the boundary conditions for the split system (see Fig. 1) $\mathscr{F}\{\mathscr{H}\}$ and $\mathscr{F}\{\mathscr{H}+\mathscr{H}_{\rm seam}\}$ have identical bulk and surface contributions which therefore cancel each other in Eq. (2.7). Moreover, corrections to the critical surface or interfacial tensions due to *finite* M [21] cancel as well, provided effects due to the finite mesh size of the lattice can be neglected. By evaluating the right-hand side (rhs) of Eq. (2.7) for sufficiently large lattices we thus probe the critical finite-size part of the free energy *directly*. Note, that due to the short-ranged nature of the interaction in the Potts model and in the Ising model according to Eqs. (2.1) and (2.3) the van der Waals contribution to Eq. (1.4) is replaced by a contribution containing *exponentially* small terms.

If $\Delta_{a,b}$ denotes the Casimir amplitude for boundary conditions of type a and b imposed on the two boundaries of the system, respectively, the left-hand side (lhs) of Eq. (2.7) can be directly related to $\Delta_{a,b}$ and the Casimir amplitude $\Delta_{\rm per}$ for periodic boundary conditions. Using the standard decomposition of the free energy in a slab geometry (see Eq. (1.2) and Ref. [9]) we have for sufficiently large M,L and in the limit of vanishing aspect ratio s

$$\mathscr{F}\{\mathscr{H}+\mathscr{H}_{\rm seam}\}-\mathscr{F}\{\mathscr{H}\}=k_BT_c(\Delta_{a,b}+2\Delta_{\rm per})M/L \quad (2.8)$$

in $d=2$ and

$$\mathscr{F}\{\mathscr{H}+\mathscr{H}_{\rm seam}\}-\mathscr{F}\{\mathscr{H}\}=k_BT_c(3\Delta_{a,b}+4\Delta_{\rm per})M^2/L^2 \quad (2.9)$$

in $d=3$. By comparing Eqs. (2.8) and (2.9) with Eq. (2.7) we find the Casimir amplitudes are given by the thermodynamical average on the rhs of Eq. (2.7), which is directly accessible in a Monte Carlo simulation. However, one must keep in mind, that Eqs. (2.8) and (2.9) are only *asymptotically* valid for large systems (see Secs. III and IV). Note, that as in Ref. [19] the Casimir amplitude $\Delta_{\rm per}$ for purely periodic boundary conditions is a directly measurable quantity. All other Casimir amplitudes require the knowledge of $\Delta_{\rm per}$.

The accurate measurement of the rhs of Eq. (2.7) requires special sampling techniques [22,23] which, in part, have already been implemented in previous investigations of related problems [18]. However, the necessity of studying large systems in order to be able to take advantage of Eqs. (2.8) and (2.9) demands both efficient Monte Carlo algorithms and data analysis techniques. These techniques are available in the form of the Wolff algorithm [24] for the Monte Carlo part and in the form of the optimized multiple histogram analysis [25] for the data analysis part of this investigation. The Wolff algorithm is the most efficient way to limit the growth of the integrated autocorrelation time of the algorithm, which crucially enters the statistical error of all measured quantities [26]. In our case this is particularly important, because our simulation data are taken exclusively *at* the infinite-lattice critical temperature T_c where critical slowing down leads to a steep increase of the autocorrelation times of the local update algorithms like the heat bath or the Metropolis algorithm with the lattice size. The implementation of the Wolff algorithm for the splitting process described above is straightforward, because each intermediate Hamiltonian $\mathscr{H}_\lambda$ [see Eqs. (2.1), (2.5), and (2.6)] describes a *ferromagnetic* spin model. According to Eq. (2.7) the quantity to be measured is the seam energy $E_{\rm seam}=\mathscr{H}_{\rm seam}\{\sigma\}$ associ-

ated with the seam Hamiltonian. It is evident from Eq. (2.6) that the seam energy contains both contributions resembling the energy density, which contains neighboring spins, and contributions resembling the spin-spin correlation function, which contains spins a distance $L/2$ apart. In order to deal with this mixed nature of $E_{\rm seam}$ we have employed a hybrid update scheme which consists of one Metropolis update of the entire lattice followed by a Wolff update.

The choice of the random number generator is crucial and depends on the update algorithm [27]. Shift register generators are given by the recursion relation $X_n = X_{n-p} \oplus X_{n-q}$, where X is the computer word with, e.g. 32 bits and $\oplus$ denotes the bitwise XOR operation. These generators are fast and easy to implement, but for smaller lags p, like in the R250 ($p=250$, $q=103$), they cause large systematic errors if they are used with the Wolff algorithm [27]. For the hybrid update scheme used here these systematic deviations are much smaller and become even unnoticeable, if a shift register generator with a larger lag is used [27,28]. We have therefore chosen the R1279 ($p=1279$, $q=1063$) shift register generator for our simulation. In order to test the R1279 for our Monte Carlo algorithm we have also implemented the linear congruential (CONG), the subtract with carry (SWC), and shift register generators with a smaller (R250) and a larger lag (R3217) for comparison, where $p=3217$ and $q=2641$ in the latter.

In order to obtain an accurate measurement of the rhs. of Eq. (2.7) we consider a sequence of Hamiltonians $\mathscr{H}_\lambda$ for typically 9–12 values of $\lambda (0 \leqslant \lambda \leqslant 1)$ in $d=2$ and typically 25 values of λ in $d=3$. For each value of λ a histogram of the seam energy $E_{\rm seam}$ is recorded and written to a file for later analysis using the optimized multiple histogram analysis described in Ref. [25]. The values for λ are chosen such that the histograms $N_\lambda(E_{\rm seam})$ of the seam energy for the successive values of λ have sufficient overlap for the multiple histogram method to converge properly (for examples, see Secs. III and IV). As a result we obtain the normalization factor $z(\lambda)$ for each individual histogram, from which the *relative* normalization of two histograms N_{λ_1} and N_{λ_2} can be inferred to be [25]

$$z(\lambda_2)/z(\lambda_1) = \langle \exp[-(\lambda_2-\lambda_1)\mathscr{H}_{\rm seam}/k_B T_c] \rangle_{\mathscr{H}_{\lambda_1}}. \quad (2.10)$$

The rhs of Eq. (2.7), and therefore the desired Casimir amplitudes, follow from Eq. (2.10) for $\lambda_1=0$ and $\lambda_2=1$. The autocorrelation times needed for the analysis are estimated from the time displaced autocorrelation function $\langle E_{\rm seam}(t) E_{\rm seam}(0) \rangle_{\mathscr{H}_\lambda}$ as a function of the split parameter λ. The variance of the resulting density of states $W(E_{\rm seam})$ determines the statistical error of the Casimir amplitudes [25].

The simulations have been performed on a cluster of IBM RS/6000 workstations and using a hybrid, parallel code on an IBM SP2 computer at the University of Georgia.

III. CASIMIR AMPLITUDES FOR THE $d=2$ POTTS MODEL

In two dimensions the q-state Potts universality class incorporates various critical phenomena, which for $q=2$ (Ising universality class), $q=3$, and $q=4$ are realized by the order-disorder transitions in adsorbed monolayers [29]. The Ising model ($q=2$) has been solved rigorously on finite rectangular lattices with arbitrary aspect ratios in the case of periodic boundary conditions [30]. For the three-state Potts model, however, much less rigorous information is available because exact solutions only exist in the thermodynamic limit and *at* criticality [15]. The four-state Potts model is known to have logarithmic corrections to scaling [31] which also affect the critical finite-size behavior [32].

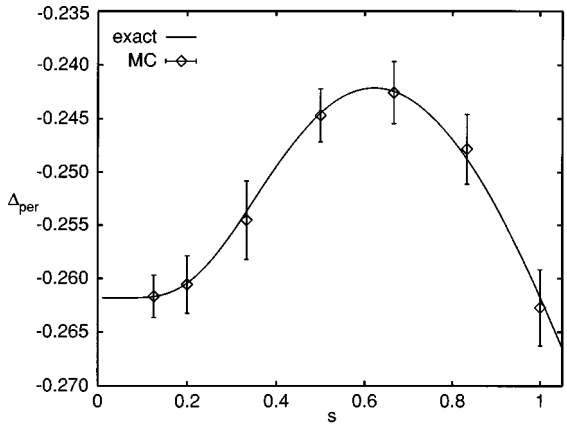

FIG. 2. Casimir amplitude $\Delta_{\rm per}$ (periodic boundary conditions) as a function of the aspect ratio s for $q=2$. The solid line shows the exact result in the continuum limit (see main text) and the symbols indicate Monte Carlo results for $\frac{1}{8} \leqslant s \leqslant 1$. The relative statistical error is $<1.5\%$ for all s. The size of each error bar represents one standard deviation.

For $q=2$ and $q=3$ the Casimir amplitudes Δ can be rigorously obtained from the conformal field theory [13] which yields a continuum description and a classification of the corresponding lattice models through their conformal anomaly number c. The critical q-state Potts model is characterized by $c=\frac{1}{2}$ for $q=2$ and by $c=\frac{4}{5}$ for $q=3$ [33]. Due to its borderline nature the critical four-state Potts model is characterized by $c=1$ [34] which is also the conformal anomaly number for the critical one-component Gaussian model in $d=2$.

The finite-size behavior of the free energy of the critical q-state Potts model confined to an infinite strip geometry can only be characterized by the Casimir amplitudes in the continuum limit. Monte Carlo studies, however, are always restricted to completely finite lattices. Therefore in a first step a lattice size L must be found which is large enough to enable us to neglect the effects of the finite mesh size of the lattice on the free energy. Secondly, a lattice size $M > L$ must be found which brings our finite rectangular geometry sufficiently close to the infinite strip limit. In order to accomplish this we resort to the case $q=2$ and periodic boundary conditions so that we can take advantage of the exact expression for the free energy given in Eq. (3.37) of Ref. [30]. We use this result to evaluate Eq. (2.8) for $\Delta_{a,b} = \Delta_{\rm per}$ in the continuum limit $M, L \to \infty$ at an arbitrarily fixed aspect ratio $s = L/M$. This defines $\Delta_{\rm per}$ as a function of the aspect ratio s and we use our Monte Carlo algorithm (described in Sec. II) to probe this function at fixed L for several values of $M \geqslant L$, i.e., for several values of $s \leqslant 1$. The result for $L=40$ and $40 \leqslant M \leqslant 320$ is displayed in Fig. 2. The solid line shows the

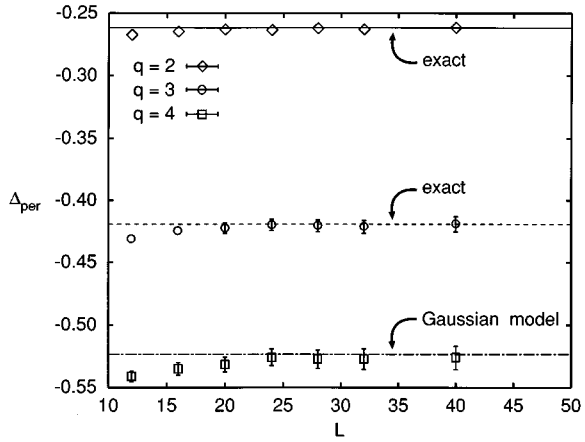

FIG. 3. Casimir amplitude Δ_{per} for fixed aspect ratio $s=\frac{1}{8}$ as a function of L for $q=2$ (diamond), $q=3$ (circle), and $q=4$ (square). The theoretical values are indicated by the solid line ($q=2$), the dotted line ($q=3$), and the dash-dotted line ($q=4$) [see Eqs. (3.1) and (3.2)]. Error bars are not displayed whenever they are smaller than the symbol sizes. The size of each error bar represents one standard deviation.

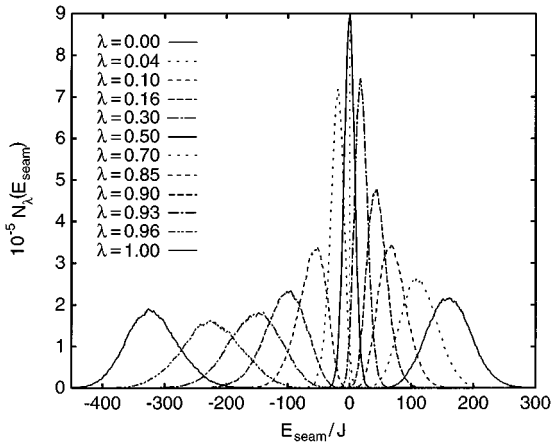

FIG. 4. Histograms $N_\lambda(E_{\text{seam}})$ for $q=4$, $M\times L=320\times 40$, and periodic boundary conditions. The seam energy E_{seam} is given in units of the coupling constant J. From *right* to *left* N_λ is shown for increasing λ. Note the sensitive dependence of the *shape* of N_λ on λ.

exact continuum limit obtained from Eq. (3.37) of Ref. [30] and our Monte Carlo estimates are indicated by the diamond shaped symbols. After equilibrating the system for 10^4 hybrid Monte Carlo steps (i.e., >100 autocorrelation times) for each of the 9,...,12 histograms (see below), we have used a total of 7.2×10^5 hybrid Monte Carlo steps per histogram for measurements for each system size. The excellent agreement with the exact result for all aspect ratios leads us to the conclusion that $L=40$ is sufficient to reach the continuum limit within our error bars. Furthermore, the aspect ratio $s=1/8$ is sufficiently close to the infinite strip limit $s=0$ within our error bars.

In order to study the decay of finite mesh size effects on Δ_{per} with increasing L, we fix the aspect ratio of our rectangular geometry to $s=1/8$ and estimate Δ_{per} for a sequence of lattices with $12\leqslant L\leqslant 40$ with periodic boundary conditions for $q=2$, 3, and 4. We use the same number of histograms and the same amount of Monte Carlo steps as above, where the system is always equilibrated for >100 autocorrelation times for each histogram. The resulting estimates for Δ_{per} are displayed in Fig. 3. The horizontal lines indicate the analytical results for Δ_{per} from conformal field theory for an infinite strip. For $q=2$ (solid line) and $q=3$ (dashed line) these are exact [13], whereas for $q=4$ (dash-dotted line) the corresponding amplitude Δ_{per} for a one-component critical Gaussian model in $d=2$ [3] is shown. Within the error bars, which are not displayed in Fig. 3 whenever they are smaller than the symbol sizes, our estimated values for Δ_{per} approach the theoretically expected values monotonically from below as L increases. These theoretical values lie clearly inside the error bars of our Monte Carlo estimates if $L\geqslant 28$ for $q=2$ and if $L\geqslant 24$ for $q=3$ and $q=4$. Logarithmic corrections to the critical finite-size behavior of the free energy for $q=4$ [32] cannot be detected in our data within the error bars.

From conformal field theory the Casimir amplitudes Δ_{per} are given by [35]

$$\Delta_{\text{per}}=-\frac{\pi}{6}c, \tag{3.1}$$

where c is the conformal anomaly number. Taking the averages of the estimates for Δ_{per} for $L\geqslant 28$ ($q=2$) and $L\geqslant 24$ ($q=3,4$), respectively, Eq. (3.1) can be used to obtain the conformal anomaly number c for the critical q-state Potts model from our Monte Carlo data. We obtain the following results:

$$\begin{aligned} c&=0.5009\pm 0.0020 \quad (c=\tfrac{1}{2}[33]), \quad q=2,\\ c&=0.8023\pm 0.0048 \quad (c=\tfrac{4}{5}[33]), \quad q=3,\\ c&=1.0060\pm 0.0074 \quad (c=1[32,34]), \quad q=4, \end{aligned} \tag{3.2}$$

where the theoretically expected values are shown in parentheses for comparison. Equation (3.2) demonstrates that our Monte Carlo algorithm can be used to obtain the conformal anomaly number of a critical lattice model from the Casimir effect for periodic boundary conditions, once the critical point in question has been identified. The numerical accuracy of the above Monte Carlo estimates, however, is not as good as the accuracy of corresponding estimates obtained from numerical transfer matrix calculations for the q-state Potts model [35]. The conformal anomaly number can also be determined by analyzing the two-point correlation function of the energy density. This has been done previously for the continuous spin Ising model by a Monte Carlo simulation [36].

In order to illustrate the way the histograms $N_\lambda(E_{\text{seam}})$ have been positioned with respect to the split parameter λ, we show a typical histogram distribution for $q=4$ and periodic boundary conditions in Fig. 4. The system size is $M\times L=320\times 40$, which is the largest size used in the above studies. The histograms N_λ are normalized to the number of entries which is the same for each histogram. Note, that the *shape* of N_λ changes significantly with λ, which increases from *right* to *left* in Fig. 4. According to Eq. (2.6) the range of seam energies E_{seam} to be covered increases linearly with

M so that the number of histograms has to be increased with growing M in order to maintain sufficient overlap between neighboring histograms for the multiple histogram method to converge properly. Insufficient overlap between the histograms results in slow convergence and systematic errors in the normalization factors $z(\lambda)$ and, by virtue of Eq. (2.10), in the Casimir amplitudes. In fact, for the 320×40 lattice the number of histograms can be reduced from 12 (shown in Fig. 4) to 9 without affecting the resulting estimates for $\Delta_{\rm per}$ noticeably within the error bars. The corresponding histogram distributions for $q=2$ and $q=3$ differ only slightly from the one shown in Fig. 4 so we do not reproduce them here.

We now turn to another kind of closed boundary conditions, which we will call *cyclic* in the following discussion. By cyclic boundary conditions we mean that the spins $s(x,1)$ and $s(x,L)$ are still treated as nearest neighbors, but this time $s(x,1)$ is ferromagnetically coupled to $s(x,L)+k \pmod q$ rather than to $s(x,L)$ itself, where k denotes an integer shift parameter. For a q-state Potts model the shift parameter k can take the values $k=0,1,\ldots,q-1$ and the corresponding Casimir amplitude will be denoted by $\Delta_{{\rm cyc},k}$. Clearly $\Delta_{{\rm cyc},0}\equiv\Delta_{\rm per}$ and for $(q,k)=(2,1)$ we have the equivalent of *antiperiodic* (aper) boundary conditions for a spin-$\frac{1}{2}$ Ising model. For $q=3$ we have the two choices $k=1$ and $k=2$ apart from periodic boundary conditions. However, these two choices are rendered equivalent by relabeling the Potts states according to $1\rightarrow3,3\rightarrow2,2\rightarrow1$, and therefore $\Delta_{{\rm cyc},1}=\Delta_{{\rm cyc},2}$ for $q=3$ [13]. For $q=4$ the choices $k=1$ and $k=3$ are equivalent by an analogous argument giving $\Delta_{{\rm cyc},1}=\Delta_{{\rm cyc},3}$ in this case. Setting $k=2$, however, maps the four Potts states onto themselves according to $1\leftrightarrow3,2\leftrightarrow4$, which is not equivalent to the former two choices of k and therefore the relation of $\Delta_{{\rm cyc},2}$ to the other amplitudes for $q=4$ remains to be determined.

Unlike periodic boundary conditions cyclic boundary conditions for $k>0$ introduce an interior *interface* into the system which has a critical finite-size behavior of its own. Although the interfacial tension is a part of the finite-size contribution to the free energy in a strip or a slab geometry by definition [see Eq. (1.2)], the inevitable finiteness of our lattices introduces finite-size corrections due to finite M to the interfacial tension [21] which need to be compensated. It is for this reason that, by virtue of Eq. (2.8), only $\Delta_{{\rm cyc},k}+2\Delta_{\rm per}$ can be measured directly rather than $\Delta_{{\rm cyc},k}$ itself (see also Sec. II).

As in our Monte Carlo studies for periodic boundary conditions (see Fig. 3) we fix the aspect ratio to $s=\frac{1}{8}$ and measure $\Delta_{{\rm cyc},1}+2\Delta_{\rm per}$ for a sequence of lattices with $12\leqslant L\leqslant40$ and for $q=2,3,4$ from a multiple histogram analysis of 11 histograms (see below). The number of Monte Carlo steps per histogram for equilibration (>100 autocorrelation times) and measurement remain the same as in the case of periodic boundary conditions. For each L we obtain an estimate for $\Delta_{{\rm cyc},1}$ from the previously made estimate for $\Delta_{\rm per}$ for the same value of L. This allows us to study the decay of finite mesh size effects of the lattice on $\Delta_{{\rm cyc},1}$ with increasing L. The result is displayed in Fig. 5. For $q=2$ and $q=3$ the exact values of $\Delta_{{\rm cyc},1}$ [13] in an infinite strip geometry are indicated by the solid and the dashed line, respectively. Within the error bars, the estimated values approach the exact ones monotonically from above as L increases. For $q=4$ and the

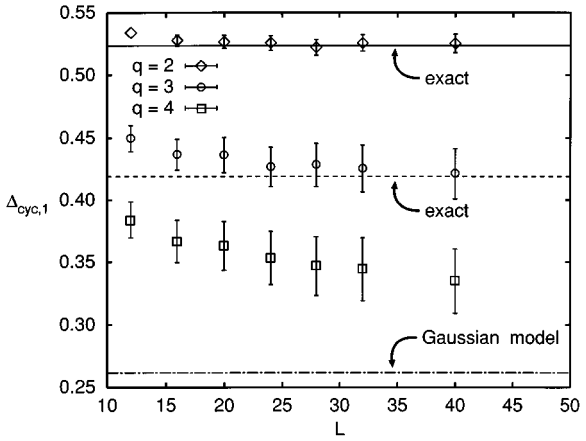

FIG. 5. Casimir amplitude $\Delta_{{\rm cyc},1}$ for the fixed aspect ratio $s=\frac{1}{8}$ as a function of L for $q=2$ (diamond), $q=3$ (circle), and $q=4$ (square). Theoretical values are indicated by the solid line ($q=2$,[13]), the dotted line ($q=3$,[13]), and the dash-dotted line ($q=4$, one-component Gaussian model). Error bars are not displayed whenever they are smaller than the symbol sizes (representing one standard deviation).

Gaussian model, however, the situation is different. The exact result $\Delta_{{\rm cyc},1}\equiv\Delta_{\rm aper}=\pi/12$ for a one-component critical Gaussian model in $d=2$, which is indicated by the dash-dotted line in Fig. 5, remains far outside the error bars for any value of L. Our Monte Carlo data are fully consistent with the standard finite-size behavior according to Eq. (2.8) within the error bars, logarithmic corrections to Eq. (2.8) cannot be identified. For $(q,k)=(4,1)$ the Gaussian model with *antiperiodic* boundary conditions does not represent the critical finite-size behavior of the Potts model.

Averaging the Monte Carlo estimates for $\Delta_{{\rm cyc},1}+2\Delta_{\rm per}$ for $L\geqslant28$ and combining them with the corresponding estimates for $\Delta_{\rm per}$ we obtain our final estimates for $\Delta_{{\rm cyc},1}$. The results together with estimates for $(q,k)=(3,2)$ and $(q,k)=(4,2)$ and $(4,3)$ are summarized in Table I. The exact results for $q=2$ and $q=3$ [13] and the corresponding results for the critical one-component Gaussian model for $q=4$ are given for comparison. The Casimir effect for the four-state Potts model with cyclic boundary conditions is independent of k for $k\geqslant1$ within our error bars. The amplitudes given in Table I for $k\geqslant1$ must be considered as *effective* amplitudes, because they are derived from Eq. (2.8), where logarithmic corrections have been disregarded.

We close this section with a few comments on the histogram distribution for cyclic boundary conditions with respect to the split parameter λ. It has already been pointed out, that the histograms must be carefully positioned in order to guarantee sufficient overlap between neighboring histograms. It turns out, that this positioning of the histograms is also quite sensitive to the boundary conditions. An example for $(q,k)=(4,1)$ is shown in Fig. 6, where the typical histogram distribution for cyclic boundary conditions and $M\times L=320\times40$ is displayed. Compared to Fig. 4 the histograms are almost symmetrically arranged around $\lambda=0.5$ and are not as sharply peaked near $\lambda=0.5$. Furthermore, the histograms can be more evenly spaced with respect to λ in order to cover the entire range of seam energies with sufficient overlap be-

TABLE I. Casimir amplitudes Δ for the critical q-state Potts model confined to a strip in $d=2$ with periodic and cyclic boundary conditions (see main text). For $q=2$ and $q=3$ the exact results [13] are shown for comparison in parenthesis. For $q=4$ the corresponding amplitudes for a critical Gaussian model are displayed.

q	Δ_{per}	$\Delta_{\mathrm{cyc},1}$	$\Delta_{\mathrm{cyc},2}$	$\Delta_{\mathrm{cyc},3}$
2	-0.2623 ± 0.0010	0.5242 ± 0.0039		
	$\left(-\frac{\pi}{12}\simeq-0.2618\right)^{a}$	$\left(\frac{\pi}{6}\simeq0.5236\right)^{a}$		
3	-0.4201 ± 0.0025	0.4257 ± 0.0103	0.4248 ± 0.0101	
	$\left(-\frac{2\pi}{15}\simeq-0.4189\right)^{a}$	$\left(\frac{2\pi}{15}\simeq0.4189\right)^{a}$	$\left(\frac{2\pi}{15}\simeq0.4189\right)^{a}$	
4	-0.5268 ± 0.0039	0.3432 ± 0.0136	0.3501 ± 0.0136	0.3425 ± 0.0136
	$\left(-\frac{\pi}{6}\simeq-0.5236\right)^{b}$	$\left(\frac{\pi}{12}\simeq0.2618\right)^{b}$	$\left(\frac{\pi}{12}\simeq0.2618\right)^{b}$	$\left(\frac{\pi}{12}\simeq0.2618\right)^{b}$

[a]Ref. [13].
[b]Gaussian model.

tween subsequent histograms than for periodic boundary conditions. The number of histograms (11 in Fig. 6) can be reduced to 9 without changing the final estimates for $\Delta_{\mathrm{cyc},k}$ noticeably.

The Monte Carlo results presented above are mainly obtained from the R1279 random number generator. For both the periodic and the cyclic boundary conditions and all values of q several series of runs have been repeated using the CONG, the SWC and the R250 random number generator. The mutual deviations in the final estimates for Δ were always smaller than the statistical error.

IV. CASIMIR AMPLITUDES FOR THE $d=3$ ISING MODEL

In three dimensions the Ising universality class incorporates critical phenomena in the vicinity of a simple liquid-vapor critical point and it therefore has the most widespread realizations of any universality class. With respect to the Casimir effect in a wetting layer (see Sec. I) it is the relevant universality class for a film of a binary liquid mixture near the critical end point of the demixing transitions [11,12], where surface fields have to be included. Unlike its two-dimensional counterpart the nearest neighbor spin-$\frac{1}{2}$ Ising model in $d=3$ [see Eq. (2.3)] is still lacking a rigorous treatment. Therefore the Casimir amplitudes Δ can also only be estimated with uncertain numerical accuracy [9,14]. According to the results presented in the previous section, however, the prospects for the Monte Carlo algorithm presented here to substantially improve the currently known estimates for Δ in $d=3$ seem to be very good.

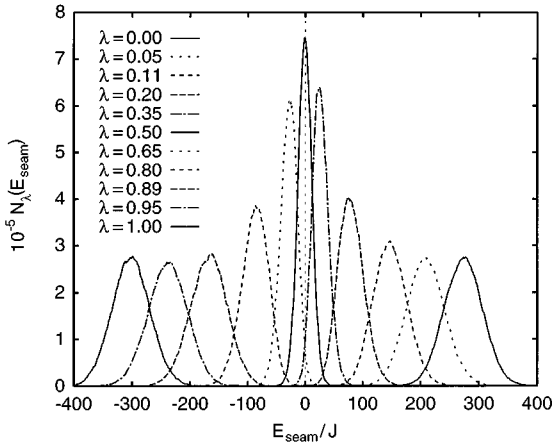

FIG. 6. Histograms $N_\lambda(E_{\mathrm{seam}})$ for $(q,k)=(4,1)$ and $M\times L=320\times40$. The seam energy E_{seam} is given in units of the coupling constant J. From *right* to *left* N_λ is shown for increasing λ. Note the difference in the dependence of the *shape* of N_λ on λ as compared to the periodic boundary conditions (see Fig. 4).

A lattice resembling an infinite slab in $d=3$ contains typically 100 times more lattice sites than its counterparts in $d=2$. In order to cope with the corresponding increase in demand for computational resources we have parallelized our hybrid algorithm in a way suitable for an IBM SP2 utilizing its high bandwidth, low latency switches for communication. The parallization scheme [37] uses four processors one of which equilibrates the system and generates a sequence of equilibrium spin configurations using the Wolff algorithm. The remaining three processors perform Metropolis updates of a previously generated configuration in order to set up histograms of the seam energy E_{seam} and measure other quantities like the energy density, the specific heat, the magnetization, and the magnetic susceptibility for control purposes. Configurations are provided by the Wolff process and sent to the Metropolis processes whenever one is ready to receive a new configuration. The idle time of the processors is minimized by adjusting the number of Wolff and Metropolis updates performed in the interval between the broadcasts of the new configurations. Typically, the Wolff process sends a new configuration every four updates and a Metropolis process performs seven updates for measurements, which yields a parallel efficiency between 75% and 85% depending on the system size.

Following the procedure described in the previous section for $d=2$, we probe the Casimir amplitude Δ_{per} for the periodic boundary conditions using Eq. (2.9) as a function of the aspect ratio $s\equiv L/M\leqslant1$ and varying L between 12 and 24.

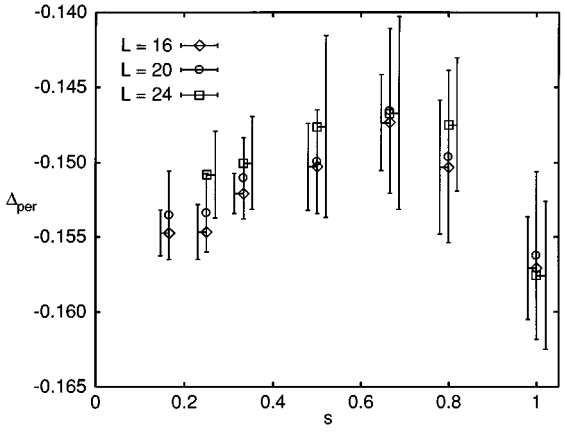

FIG. 7. Casimir amplitude Δ_{per} (periodic boundary conditions) for the Ising universality class in $d=3$ as function of the aspect ratio s for $L=16$ (diamond), $L=20$ (circle), and $L=24$ (square). The Monte Carlo results for $\frac{1}{6}\leqslant s\leqslant 1$ are displayed. The relative statistical error is $<4\%$ for all s. The error bars for $L=16$ have been moved to the left and those for $L=24$ have been moved to the right for clearity. The size of each error bar represents one standard deviation.

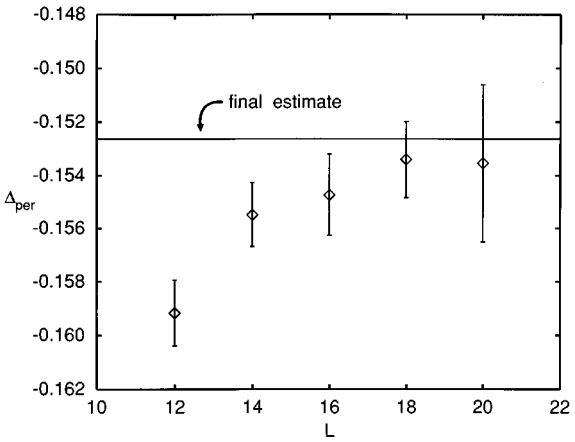

FIG. 8. Casimir amplitude Δ_{per} for the fixed aspect ratio $s=\frac{1}{6}$ as a function of L for the critical Ising model. The solid line indicates our final Monte Carlo estimate for Δ_{per} [see Eq. (4.1)]. The size of each error bar represents one standard deviation.

After equilibrating the system for 10^3 Wolff updates (typically >10 autocorrelation times), we have used a total of 1.1×10^5 Wolff updates per histogram for the measurements for each system size. In order to guarantee sufficient overlap between subsequent histograms even for the largest lattices used in this investigation, we have used 25 histograms of E_{seam} for all system sizes in the final multiple histogram analysis. As an example we show the results for $16\leqslant L\leqslant 24$ and $1/6\leqslant s\leqslant 1$ in Fig. 7. In comparison with $d=2$ (see Fig. 2), Δ_{per} does not vary as much with the aspect ratio s and, within the error bars, the infinite slab limit $s=0$ is already reached for $s=1/6$. Furthermore, Fig. 7 shows that the estimates for Δ_{per} as functions of s have already become independent of L for $L\geqslant 20$. For $L=16$ there are still traces of small systematic deviations due to finite mesh size effects present in our data. The increase in the error bars for increasing L is due to increasing autocorrelation times and decreasing overlap between neighboring histograms. Furthermore, the error bars show the tendency to increase with s (to the right in Fig. 7), because the histograms contain fewer entries for smaller values of M. The relative statistical errors are between two and four times as large as in $d=2$ which is due to both larger autocorrelation times and poorer statistics in $d=3$. Averaging the values of Δ_{per} from our Monte Carlo data obtained for $L=20$ and $L=24$ for the aspect ratios $s=1/4$ and $s=1/6$, we obtain our final estimate

$$\Delta_{per}=-0.1526\pm 0.0016 \tag{4.1}$$

for the critical Ising model in $d=3$. For comparison one obtains $\Delta_{per}\simeq -0.11$ from an ϵ expansion ($\epsilon=4-d$) up to first order in ϵ [9]. Combining a partial resummation of the ϵ expansion with an interpolation scheme using the exact result $\Delta_{per}=-\pi/12$ for the Ising (two-state Potts) model in $d=2$ one obtains the following approximate interpolation formula for Δ_{per} as a function of the spatial dimension d within the Ising universality class [9]

$$\Delta_{per}=-\pi^{-d/2}\Gamma\left(\frac{d}{2}\right)\zeta(d)\left(1-\frac{5}{4}\,\frac{4-d}{7-d}\right). \tag{4.2}$$

Note that Eq. (4.2) reproduces both the ϵ expansion to the first order for $d=4-\epsilon$ and the exact result for $d=2$. For $d=3$ Eq. (4.2) yields the estimate $\Delta_{per}\simeq -0.13$, which improves the pure ϵ-expansion result, but still remains far outside the statistical error of our Monte Carlo estimate given by Eq. (4.1).

Finally, we have studied the decay of the finite mesh size effects on our estimates for Δ_{per} with increasing L for a sequence of lattices with $12\leqslant L\leqslant 20$ at a fixed aspect ratio $s=\frac{1}{6}$ of our slab geometry. The Casimir amplitude Δ_{per} according to Eq. (2.9) as a function of L is shown in Fig. 8, the solid line indicates our estimate for Δ_{per} according to Eq. (4.1). As for $d=2$ (see Fig. 3) the estimates for Δ_{per} approach the solid line monotonically from below as L increases, but effects of the finite mesh size of the lattice decay considerably faster. For $L=16$ these effects are already smaller than the statistical error.

We close our presentation with a few comments on the typical histogram distribution in $d=3$, which we do not reproduce here. In contrast to the two-dimensional case shown in Fig. 4 the histograms N_λ can be almost evenly spaced with respect to λ. Furthermore, the shape of N_λ varies much less with λ than in $d=2$, which simplifies the positioning of the histograms considerably. In order to guarantee sufficient overlap between neighbor histograms, roughly twice as many histograms as for the corresponding two-dimensional case are required, although the range of seam energies has increased by more than an order of magnitude. Maintaining sufficient overlap, however, has become much more demanding, because the range of seam energies E_{seam} to be covered grows as M^2 in $d=3$.

V. SUMMARY AND OUTLOOK

From the basic mechanism underlying the well-known Casimir effect in electromagnetism it is clear that critical fluctuations in a confined system lead to a critical finite-size

contribution to its free energy, which is the direct analogue of the Casimir effect given by Eq. (1.1). At the critical point of the system this finite-size contribution to the free energy can be characterized by the *universal* Casimir amplitudes Δ [see Eqs. (1.2) and (1.4)], which in $d=3$ dimensions are experimentally accessible by, e.g., a wetting experiment [9]. We have presented a Monte Carlo algorithm which is capable of probing these Casimir amplitudes for a critical system confined to a strip ($d=2$) or slab ($d=3$) geometry with considerable accuracy. The statistical errors are small enough to probe the dependence of our estimates for Δ on the aspect ratio s of the lattice and the number L of lattice rows or lattice planes in $d=2$ or $d=3$, respectively.

In $d=2$ our Monte Carlo estimates of the Casimir amplitudes for the critical q-state Potts model confined to a slab geometry with periodic and cyclic boundary conditions agree very well with exact results for $q=2$ and $q=3$. For $q=4$ and periodic boundary conditions Δ_{per} agrees very well with the corresponding value for the critical one-component Gaussian model, as expected from conformal field theory (see Eq. (3.2) and Ref. [34]). For $q=4$ and cyclic boundary conditions we have extracted an *effective* Casimir amplitude $\Delta_{\mathrm{cyc},1}=\Delta_{\mathrm{cyc},2}=\Delta_{\mathrm{cyc},3}$ from Eq. (2.8), which does not match $\Delta_{\mathrm{aper}}\equiv\Delta_{\mathrm{cyc},1}$ for the critical one-component Gaussian model confined to a strip with antiperiodic boundary conditions. Logarithmic corrections to the critical finite-size behavior of the free energy, which would also appear in Eq. (2.8), remain unresolvable within our error bars.

For other boundary conditions such as the application of surface fields, which generate *surface* contributions to the free energy, the critical q-state Potts model confined to a strip geometry also provides the natural testing ground for our algorithm. The presence of these surfaces, however, enhances effects of the finite mesh size of the lattice on the free energy substantially, so that with the present version of our algorithm larger lattice sizes must be considered. In order to avoid larger lattices, the accordingly increased autocorrelation times, and the resulting additional demand for computational resources the algorithm must be modified to include, e.g., anisotropic coupling constants. Further studies with this modified version of our algorithm are currently under way.

In $d=3$ we have investigated a critical Ising model confined to a slab geometry with periodic boundary conditions for which no exact results are known. In order to deal with the drastically enhanced demand for computational resources in this case we have parallelized our algorithm in a way suitable for an IBM SP2 utilizing four processors in parallel. We have found that Δ_{per} varies only half as much with the aspect ratio than it does in $d=2$ and that the infinite slab limit is already reached for $s=1/6$. Furthermore, effects of the finite mesh size of the lattice decay faster than in $d=2$ so that the overall lattice sizes could be kept moderately small in our simulation. Existing field-theoretic estimates for the Casimir amplitude Δ_{per} for the Ising universality class in $d=3$ remain far outside the statistical error of our final Monte Carlo estimate [see Eq. (4.1)].

As far as other boundary conditions, especially those characterized by magnetized surfaces, are concerned, the situation is similar to the two-dimensional case. The presence of the surfaces requires an appropriate customization and further testing of the algorithm, which is currently under way.

ACKNOWLEDGMENTS

We gratefully acknowledge many useful discussions with A. M. Ferrenberg and K. K. Mon. One of us (M. Krech) was supported through the Feodor Lynen program of the Alexander von Humboldt Foundation. This research was also supported in part by NSF Grant No. DMR-9405018.

[1] H. B. G. Casimir, Proc. K. Ned. Akad. Wet. **51**, 793 (1948); Physica **19**, 846 (1953).
[2] J. Schwinger, L. L. DeRaad, and K. A. Milton, Ann. Phys. (N.Y.) **115**, 1 (1978).
[3] E. Elizalde, Nuovo Cimento **104**, 685 (1989).
[4] E. M. Lifshitz, Zh. Eksp. Teor. Fiz. **29**, 94 (1955) [Sov. Phys. JETP **2**, 73 (1956)].
[5] I. E. Dzyaloshinskii, E. M. Lifshitz, and L. P. Pitaevskii, Adv. Phys. **10**, 165 (1961).
[6] R. Eisenschitz and F. London, Z. Phys. **60**, 491 (1930).
[7] S. Dietrich, in *Phase Transitions and Critical Phenomena*, edited by C. Domb and J. L. Lebowitz (Academic, London, 1988), Vol. 12, p. 1.
[8] E. S. Sabisky and C. H. Anderson, Phys. Rev. A **7**, 790 (1973).
[9] M. Krech and S. Dietrich, Phys. Rev. A **46**, 1886, 1922 (1992); M. Krech, *The Casimir Effect in Critical Systems* (World Scientific, Singapore, 1994).
[10] J. O. Indekeu, J. Chem. Soc., Faraday Trans. II **12**, 1835 (1986).
[11] M. P. Nightingale and J. O. Indekeu, Phys. Rev. Lett. **54**, 1824 (1985); **55**, 1700 (1985).
[12] R. Lipowsky and U. Seifert, Phys. Rev. B **31**, 4701 (1985); R. Lipowsky, Phys. Rev. Lett. **55**, 1699 (1985).
[13] J. L. Cardy, Nucl. Phys. B **275**, 200 (1985).
[14] J. O. Indekeu, M. P. Nightingale, and W. V. Wang, Phys. Rev. B **34**, 330 (1986).
[15] F. Y. Wu, Rev. Mod. Phys. **54**, 235 (1982); R. J. Baxter, *Exactly Solved Models in Statistical Mechanics* (Academic, New York, 1982).
[16] A. Rosengren, J. Phys. A **19**, 1709 (1986).
[17] D. P. Landau, Physica A **205**, 41 (1994) and references therein.
[18] K. K. Mon, Phys. Rev. Lett. **54**, 2671 (1985); Phys. Rev. B **35**, 3560 (1987).
[19] A. D. Bruce, J. Phys. A **28**, 3345 (1995).
[20] V. Privman, P. C. Hohenberg, and A. Aharony, in *Phase Transitions and Critical Phenomena*, edited by C. Domb and J. L. Lebowitz (Academic, New York, 1991), Vol. 14, p. 1.
[21] V. Privman, in *Finite Size Scaling and Numerical Simulation of Statistical Systems*, edited by V. Privman (World Scientific, Singapore, 1990).
[22] C. H. Bennett, J. Comput. Phys. **22**, 245 (1976).
[23] G. M. Torrie and J. P. Valleau, J. Comput. Phys. **23**, 187 (1977).

[24] U. Wolff, Phys. Rev. Lett. **62**, 361 (1989).
[25] A. M. Ferrenberg and R. H. Swendsen, Phys. Rev. Lett. **63**, 1195 (1989).
[26] A. M. Ferrenberg, D. P. Landau, and K. Binder, J. Stat. Phys. **63**, 867 (1991).
[27] A. M. Ferrenberg, D. P. Landau, and Y. J. Wong, Phys. Rev. Lett. **69**, 3382 (1992).
[28] A. M. Ferrenberg and D. P. Landau (unpublished).
[29] M. Schick, in *Progress in Surface Science*, edited by S. G. Davison and W. K. Liu (Pergamon, New York, 1982), Vol. 11, p. 245.
[30] A. E. Ferdinand and M. E. Fisher, Phys. Rev. **185**, 832 (1969).
[31] L. P. Kadanoff, Phys. Rev. B **22**, 2560 (1980); M. Nauenberg and D. J. Scalapino, Phys. Rev. Lett. **44**, 837 (1980).
[32] J. L. Cardy, J. Phys. A **19**, L1093 (1986).
[33] D. Friedan, Z. Qui, and S. Shenker, Phys. Rev. Lett. **52**, 1575 (1984).
[34] P. Christe and M. Henkel, *Introduction to Conformal Invariance and its Application to Critical Phenomena* (Springer, New York, 1993), p. 146 and references therein.
[35] H. W. J. Blöte, J. L. Cardy, and M. P. Nightingale, Phys. Rev. Lett. **56**, 742 (1986).
[36] X. Wang and G. A. Baker, Jr., J. Stat. Phys. **69**, 1069 (1992).
[37] A. M. Ferrenberg (private communication).